

Machine Learning-Based Classification of Hybrid BCI Signals using Mayfly-Optimized Multiclass Weighted Random Forest

R. Shelishiyah¹, Dr. Thiyam Deepa Beeta^{*2}, M. Jehosheba Margaret³

¹Research Scholar, Department of Biomedical Engineering,
Vel Tech Rangarajan Dr. Sagunthala R & D Institute of Science and Technology
Chennai, Tamilnadu, India
e-mail: shelishiyah.raymond@gmail.com

²Associate Professor, Department of Biomedical Engineering,
Vel Tech Rangarajan Dr. Sagunthala R & D Institute of Science and Technology
Chennai, Tamilnadu, India
e-mail: thiyamdeepabeeta@veltech.edu.in

³Research Scholar, Department of Biomedical Engineering,
Vel Tech Rangarajan Dr. Sagunthala R & D Institute of Science and Technology
Chennai, Tamilnadu, India
e-mail: jehosh17@gmail.com

Abstract— The Brain-Computer Interface (BCI) technologies have excellent clinical and non-clinical uses. Among the most popular imaging methods adopted in BCI technologies is electroencephalography (EEG). But EEG signals are typically quite complicated, so analyzing them necessitates a significant amount of effort. With the help of machine learning (ML), this research investigates the feasibility of a BCI platform based on the motor imagery (MI) concept. The steps of pre-processing, feature extraction and classification are the underpinning of any conventional ML model. To train such a model, however, a large amount of data is needed. To address this gap, this work introduces a new mayfly-optimized multiclass weighted random forest (MFO-MWRF) technique that uses retrieved features as input to mitigate the need for this supplementary data. In this study, we gather a dataset of hybrid EEG and fNIRS motor imagery that can be pre-processed using a Wiener filter (WF) to filter out noisier signals without affecting the high-quality images. The characteristics are extracted using the discrete wavelet transform (DWT). The research results indicate that the proposed approach achieves the best performance compared to existing approaches for classifying motor movement images.

Keywords- Brain-Computer Interface (BCI), Electroencephalography (EEG), Wiener filter (WF), discrete wavelet transform (DWT), mayfly optimized multiclass weighted random forest (MFO-MWRF)

I. INTRODUCTION

The introduction of innovative signal processing methods in recent years has greatly increased the usefulness of BCIs. Experiments with wide scope are a wonderful way to amass the mountains of data required to test out different processing methods. It is difficult and time-consuming to collect high-quality data from a big population. To control an external device, brain-computer interface (BCI) systems aim to track and record activity in the brain's cerebral cortex. It's the brain's technique of communicating with machines through electrical impulses it creates, bypassing the need for any musculature or involvement of the spinal cord or brain stem in the process [1]. A hybrid BCI system is created by combining any two modalities. In our research, signals that were obtained utilizing a combination of fNIRS and EEG were employed for analysis. The majority of the disturbances in these signals, which are

physiological sounds that cause motion artifacts, must be removed to prepare the signal for categorization. These artifacts are often eliminated using bandpass filters [2].

A hybrid BCI system was developed using MI-BCI and transient visual evoked potentials. Controlling the amplitude of motion using the intensity of motion imaging EEG will increase the efficiency of rehabilitation by involving the neurological system of the brain directly in practice. This will enable closed-loop control, encourage active movement awareness, encourage the rehabilitation of nerve function, and encourage neuroplasticity [3]. The suggested block diagram is shown in Fig 1. Applications of BCIs are quite valuable, particularly in terms of offering patients with motor dysfunction new forms of rehabilitation. They provide a novel route for communication and control between the brain and each outer environment by obviating the need for peripheral nerve and muscle tissue. Users can connect and communicate

in new ways because of this technology. BCI systems have been employed effectively in the control of robots, intelligent homes, and electric wheelchairs [4].

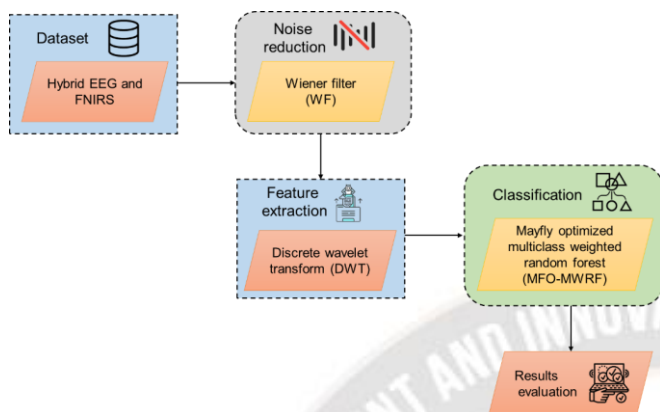


Figure 1: Block Diagram of Proposed Method

Electroencephalography (EEG) detection techniques are the most widely used in the area of BCIs because they are very safe, inexpensive, and simple to use. They often select these typical awareness activities in everyday life due to their improved ability to do mental tasks. When using the motor imaging paradigm, EEG signals from the cerebral cortex that processes movement experience event-related desynchronization/synchronization (ERD/ERS) [5]. This development for the Mayfly Optimised Multiclass Weighted Random Forest (MFO-MWRF) can improve the categorization of motor movement pictures using hybrid BCI signals.

The article's remaining sections are broken down as follows: In Section II, an overview of current research is provided; in Section III, the suggested methodology is explained in greater detail; and in Section IV, experimental data sets and simulation results are presented and discussed. The analysis is finished in Section V, which also makes recommendations for more research..

II. RELATED WORKS

The research [6] presents a smart hospital collaboration system built on the Internet of Things (IoT) and Brain-Computer Interface (BCI) that makes use of mixed signals. The paper [7] suggests a simultaneous hybrid Brain-Computer Interface (BCI) system that can decode Dual-channel EEG signals Electroencephalography (EEG) setup with sensors over the central region to detect both Motor Imagery (MI) and steady-state visually evoked potentials (SSVEP). The research [8] proposed an end-to-end semi-supervised learning system for EEG categorization and Electroencephalogram-Electromyogram (EEG-EMG) fusion analysis. The study [9] suggested linear, tensor, and p-order polynomial fusion are the three fusion methods used for the hybrid EEG and NIRS-based brain-computer interface system. The paper [10] developed and

evaluate control of home automation using a hybrid brain-computer interface (BCI) technology. BCIs have become a potential option in the last ten years for distance communication, mind reading, and medical education. The research [11] suggests a brand-new hybrid asynchronous BCI system that utilizes both blink-related electrooculography (EOG) data and EEG signal steady-state visual evoked potentials (SSVEPs). The investigation [12] proposed a distinctive channel selection method that exclusively chooses strongly associated channels from each hemisphere using the Pearson product-moment correlation coefficient. The paper [13] discussed a state-of-the-art Brain-computer interface (BCI) report focused on steady-state visual evoked potential (SSVEP), with particular emphasis on data analytics that allows for continuous, precise SSVEP detection and high information transmission rates. The research [14] conducted a 5-week longitudinal pilot study on 4 individuals with persistent hemiparesis after a stroke to assess each neurophysiological importance of Band-limited Power Time-courses (CBPT) Correlation for Motor Recovery Monitoring. The article [15] presented a variety of BCI applications, including telepresence, object grabbing, navigation, etc., that guide a humanoid robot using multi-sensor fusion and machine learning to carry out one specific job.

III. PROPOSED MODEL

Hybrid BCI signals are a computer-based system that collects brain impulses, evaluates them, and transforms them into instructions that are delivered to an output device to perform the specified operation. Experiments with the MFO-MWRF system were undertaken in this setting. With prior empirical research, the clinical and non-clinical applications of BCI signals were established.

A. Hybrid EEG and fNIRS dataset

A public dataset that concurrently captures Functional Near-Infrared Spectroscopy (FNIR) along with Electroencephalography (EEG) signals. Each piece of information was gathered from 28 right-handed competitors and 1 (14 men and 15 women) with left-handedness, with a mean lifetime and standard deviation of 28.5 and 3.7 years, respectively. The data source was then downsampled to 200 Hz and 10 Hz, respectively, the EEG and fNIRS signals. Each task, which included Baseline (BS), Mental Arithmetic (MA), Left-Hand Motor Imagery (MI), and Right-Hand Motor Imagery (MI), as a rest state condition, required each subject to complete 30 trials. Throughout the BS condition, the participant slept off without thinking. During every MA assignment, the topic was instructed into frequently a digit is subtracted numbers from three-digit numbers (for example, 384 8). For each MI assignment, participants used kinesthetic MI to

visualize their hands opening and closing. A two-second visual task introduction kicked off the study. There were EEG signals down-sampled, a shared average reference re-referenced, and then 0.5–50 Hz filtered. There were EEG signals down-sampled a frequent example of the average, 120 Hz was re-referenced before being filtered at 0.5–50 Hz. Artifacts from Electrooculography (EOG) were then eliminated using Independent Component Analysis (ICA). MI dataset and MS dataset Right-hand MI and left-handed MI are considered. We clipped instantaneous BCI performance, 3 s of EEG also fNIRS data were collected using a 1-s time step. rather than utilizing a 10-second task time for network training. There were 1,740 trials overall for each dataset (29 subjects 30 trials 2 tasks), making the size of the EEG and fNIRS signals 30 360 (channel time) and 36 30 (channel time), respectively.

B. Wiener Filter

The Wiener filter employs spectral characteristics of the signal-to-noise ratio is favorable while viewing both as linear stochastic processes features.

With coefficients W_K , this linear filter is applied to the predicted signal. The input signal, $e(k)$ include noise, $p(k)$.

$$e(k) = f(k) + p(k) \quad (1)$$

A should be the output signal, $y(n)$ precise estimation off(k). Therefore, the appropriate error signal should $x(n)$ be as little as possible. The adaptive method attempts weight adjustment W_k such as to the fact that the mean square error is kept to a minimum.

$$x = \min(x(n)^2) \quad (2)$$

$$e(k) = p(k) - f(k) \quad (3)$$

The value of y is determined by the following equation using a discrete Wiener filter with k taps (n),

$$p(k) = \sum_{n=0}^{K-1} T_n(f(k-n) * v(k-n)) \quad (4)$$

The most important characteristic of the Wiener filter is the equation of the Wiener-Hopf, which determines perfect weights,

$$\sum_{r=0}^{n-1} T_{0r_{lee}}(n-1) = l_{ef}(-r) \quad (5)$$

Where $W_{00}, W_{01}, \dots, W_{0n-1}$ represent the filter's ideal tap weight values, l_{ee} represents $e(k)$ autocorrelation function, and l_{ef} represents $x(n)$ and cross-correlation function between $e(k)$ and $f(k)$.

C. Discrete Wavelet Transform

A mathematical method for converting a picture into a series of discrete wavelets is known as the DWT pyramidal sub-images. The analysis of a signal into short waves of changing frequency and length is crucial to the transformation. Qualities are typical of waves in the wavelet range. Parameters of wavelet transformations that once referred to a specific place

become less accurate. By applying a reverse wavelet transformation to these coefficients, the original signal may be recreated in its entirety. The signals may be series produced by a mother wavelet representation of a square-integrable function. Since the Short-time Fourier Transform (STFT) window's length is fixed, it is unable to identify the frequency of EEG signals that fluctuate erratically in the temporal domain. We can easily analyze time domain and frequency domain signals in their raw form since the mother wavelet was able to dilate and translate the represented original signals.

$$TW(\alpha, 1) = \frac{1}{\sqrt{\alpha}} \int_{-\infty}^{+\infty} d(w) * \varphi\left(\frac{w-1}{\alpha}\right) fw \quad (6)$$

$$\varphi(e) = x^{-e^2} \cos\left(\pi \sqrt{\frac{2}{2}} e\right) \quad (7)$$

Feature A may be derived from the input signal B using the equation (6).

The dilation property is represented by $d(w)$, whereas the translation property is represented by TW . The wavelet function is denoted by the letter B . In this case, the Morlet wavelet is substituted for the wavelet in equation (7).

$$\Delta w = \sqrt{\frac{\int_{-\infty}^{\infty} (w-w_0)^2 |\varphi(w)|^2 fw}{\int_{-\infty}^{\infty} |\varphi(w)|^2 fw}} \quad (8)$$

$$\Delta \omega = \sqrt{\frac{\int_{-\infty}^{\infty} (\omega-\omega_0)^2 |\varphi(\omega)|^2 f\omega}{\int_{-\infty}^{\infty} |\varphi(\omega)|^2 f\omega}} \quad (9)$$

$$\omega_0 = \sqrt{\frac{\int_{-\infty}^{\infty} \omega |\varphi(\omega)|^2 f\omega}{\int_{-\infty}^{\infty} |\varphi(\omega)|^2 f\omega}} \quad (10)$$

$$w_0 = \sqrt{\frac{\int_{-\infty}^{\infty} w |\varphi(w)|^2 fw}{\int_{-\infty}^{\infty} |\varphi(w)|^2 fw}} \quad (11)$$

The raw EEG signals' original features to be preserved, it is crucial to choose the appropriate wavelet. It is straightforward to determine the wavelet's characteristics by multiplying the two variables A and B in equations (7) and equations (8), which correspond to the time and frequency domains, respectively. Equations (9) and (11) provide us with t_0 and 0 . (10). Thus, the time-frequency trade-off allows the WT algorithm to achieve great resolution.

D. Mayfly Optimized Multiclass Weighted Random Forest

Along with introducing the Particle Swarm Optimization (PSO) and Mayfly Optimized (MO) algorithms, we would also present the skeletal approach to the MO algorithm in this study. In addition, investigations based on simulations would be conducted to confirm the potential. The following equations might be used by users of the MO method to update their positions:

$$v_o(w+1) = v_o(t) + g_1 l_1 [e_{j_o} - e_o(w)] + g_2 l_2 [e_c - e_o(w)] \quad (12)$$

$$v_o(t+1) = e_o(w) + v_o(w) \quad (13)$$

Where A represents the velocity of the *i*th agent in the current iteration *t* and the previous iteration *t*+1, and B represents random variables. In the current iterations, C represents the greatest trajectory in history up to and including the *i*-th iteration, while D represents the best prospects globally. E stands for its current and future locations in the iteration.

The results of extensive simulations demonstrated that individuals' locations in the Gauss distribution A would be updated after a very large number of simulation iterations. Individuals in the MO algorithm might also use the following formulae to adjust their positions:

$$v_o(t + 1) = \begin{cases} \frac{e_{j,o} + e_c}{2} + l_3 |e_{j,o} - e_c| l_4 > 0.5 \\ \text{traditional} l_4 > 0.5 \end{cases} \quad (14)$$

Two arbitrary numbers, A and B, are used here. The remainder of the regulating variables and equations would be implemented in the standard fashion.

E. Multiclass Weighted Random Forest

A binary classification issue with $i \in \{1, \dots, n\}$ should be considered $\hat{P}_{oh} \in \{0, 1\}$ predictor variables in the training sample (D), and $X_1 - X_p$, and a class variable $k \in \{1, \dots, p\}$. Finding a model that predicts the \hat{P}_{oh} values derived from new X values is the key goal.

The Random Forest method applies the bagging strategy to each decision tree and employs *K*tree fresh training datasets p_j (also known as In-bag sample; further abbreviated as INB) (base learner). Results in the possibility of some observations can be duplicated. Electronics 2020 is often projected to make up 9996 of every 20 samples, or around 63.2% of the unique observations; the remaining observations are categorized as belonging to referred to as the "Out-of-Bag sample" (further denoted as OOB). Each applicant experiences a learning break; the RF method incorporates an extra sampling step known as a Random Decision Tree (RDT). The selection is made among the traits at random. To employ floor *p* features in each split for a classification issue with *p* features.

$$\hat{P}_o^{LD} = \sum_{h=1}^{Ktree} O[\hat{P}_{oh} > 0.5] \quad (15)$$

Where \hat{P}_{oh} stands for probability and *o* serves as an indication that each *j*th tree will assign to the other observation. The aforementioned method relies on a majority of a predetermined threshold set at 0.5, which may not always be the best choice.

Therefore, to increase flexibility (and to be more aware of any possible deviations from the anticipated outcome), the formula below is used:

$$\hat{P}_o^{LD} = \frac{1}{Ktree} \sum_{h=1}^{Ktree} \hat{P}_{oh} \quad (16)$$

This, represents into straightforward of each tree's probability, averaged.

Although tree aggregation and performance-based weights are used, they applied the standard RF technique to generate the

forest's trees. We focused on weighing the probability derived from each forest tree such that the weights of the better-performing trees were higher:

$$\hat{P}_o^{LD} = \frac{1}{Ktree} \sum_{h=1}^{Ktree} \hat{P}_{oh} * w_h \quad (17)$$

The same set of data that was used to determine the weights (as was done in would bias prediction error assessment) would be unfair since they are based on how well the particular/distinct tree performs. As a result, estimations of each tree's predictive power are computed weights may then be calculated using the INB and OOB data.

$$\theta = f(AUC_{INB}, AUC_{OOB}) = -\alpha |AUC(t^{obs})_{INB} - AUC_{OOB}| + (1 - \alpha) AUC(t^{obs})_{OOB} \quad (18)$$

This approach evaluates each tree's performance. It utilizes the supplied weight computed based on findings from the Out-of-Bag sample instead of using 1 for the above case since Such weights are implicitly supported by weighted AUC.

$$t_o^{obs} = \frac{1}{OOB} \sum_{h \in OOB} |P_{oh} - \hat{P}_{oh}| \quad (19)$$

The example is essentially disregarded if, for example, If $\text{obs } I = 0$, then each tree correctly predicted the class (which indicates that each tree accurately predicted the class). Therefore, each misclassified instances have a greater impact on a particular tree's ultimate performance.

Assuming that $\hat{P}_{oh} \in \mathbb{R}$ is the projected result for each observation; to estimate the weighted AUC, let's consider the sets of positive examples $\Gamma_0 = i: \hat{P}_{oh} = 0$ and negative instances ($0 = h \hat{P}_{oh}$). Cases Formula (18). The total beneficial weight is thus equal to $W_1 = \sum_{i \in \Gamma_1} \omega_i^{obs}$ while total negative weight is equal to $W_0 = \sum_{i \in \Gamma_0} \omega_i^{obs}$ additionally, established the following thresholding function: $t_\tau: \mathbb{R} \rightarrow \{0, 1\}$ for any threshold *R*, such as:

$$w_\tau(\hat{P}) = \begin{cases} 1, \hat{P} \geq \tau \\ 0, \hat{P} < \tau \end{cases} \quad (20)$$

This rate of weighted false positives is determined just as follows using the formula shown above:

$$FPR(\tau) = \frac{1}{T_0} \sum_{o \in \tau_0} O[w_\tau(\hat{P}_o) \neq 0] t_o^{obs} \quad (21)$$

Where, *T* is the indicator function, which is 1 in all other cases, and 0 if the prediction is correct. However, the weighted true positive rate is described as follows:

$$TPR(\tau) = \frac{1}{T_1} \sum_{o \in \tau_1} O[w_\tau(\hat{P}_o) = 1] t_o^{obs} \quad (22)$$

The graphing of FPR(*R*) and TPR(*R*) for all thresholds results in the creation of the weighted ROC curve. To produce the weighted AUC metric using the trapezoid rule (integral), and it is especially accurate for calculating the definite integral of periodic functions.

$$t_h = \frac{(Ktree - l_h + 1)^y}{\sum_{n=1}^{Ktree} (Ktree - l_n + 1)^y} \quad (23)$$

The implementation could imply that this approach only works with Random Forest. It may, however, be used for any ensemble made up of any *j* basic model type.

IV. RESULT EVALUATION

The suggested MFO-MWRF strategy's quality is examined in-depth using comparison and assessment of the results. The efficiency and accuracy of a suggested approach are compared to those of contemporary methods like the Deep Neural Network (DNN), Two-stream Convolutional Neural Network (TSCNN), and Convolutional Neural Network+ Recurrent Neural Network (CNN+RNN) to show that it is effective. The estimated Precision, Accuracy, F1-Score, and Recall are shown in the result for the provided approach.

A. Accuracy

Accuracy is determined by contrasting the number of forecasts and adjustments. Using the following equation 24,

$$Accuracy = \frac{\text{Number of correct predictions}}{\text{Total number of predictions}} \quad (24)$$

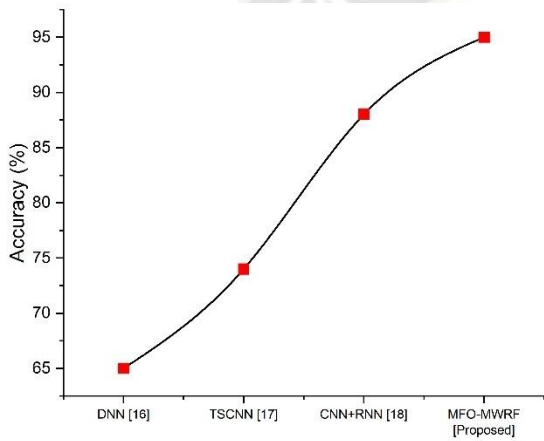


Figure 2: Accuracy

Fig 2 shows the accuracy of the proposed system. The accuracy of consumption forecasting in current systems and the suggested system is indicated. While the suggested system achieves the proposed 95% accuracy, DNN has obtained 50%, TSCNN has gained 75%, and CNN+ANN has attained 85%. It demonstrates that the suggested course of action is more successful than the existing one

B. Precision

Precision is the percentage of successfully predicted positive observations among all predicted positive observations.

$$Precision = \frac{R_o}{R_o + D_o} \quad (25)$$

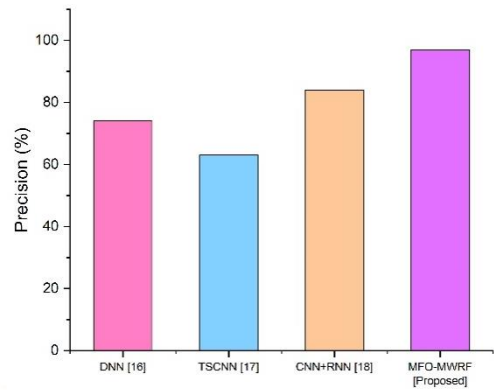


Figure 3: Precision

Fig 3 shows the precision of the proposed system. The suggested system and current systems' predictions of precision usage are discussed. While DNN has a 50% precision, TSCNN has a 75% precision, CNN+RNN has an 85% precision, and the suggested system has a 95% precision. It demonstrates that the suggested strategy is more successful than the current one.

C. Recall

Recall that compared to all observations in the class, it represents the percentage of positively anticipated observations that occurred.

$$Recall = \frac{R_o}{R_o + D_s} \quad (26)$$

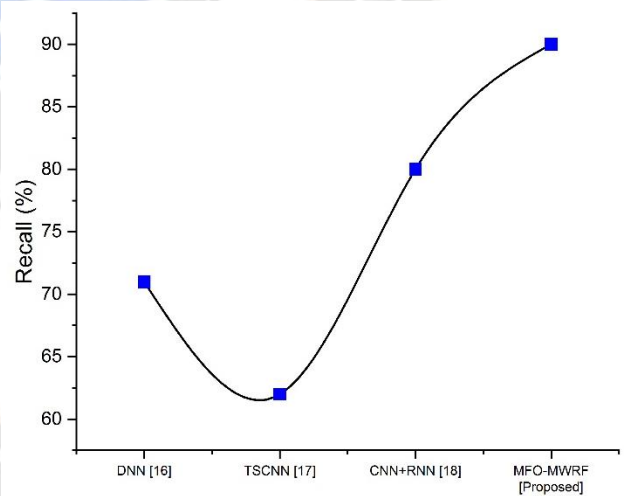


Figure 4: Recall

Fig 4 shows the Recall of the proposed system. Recall consumption forecasts for both the current system and the suggested system are shown. The suggested method achieves 95% recall compared to 50% for TSCNN, 75% for DNN, and 85% for CNN+RNN. It demonstrates how successful the suggested strategy is than the current one.

D. F1-Score

F1-score may be characterized as a weighted average of recall and accuracy. The F1 score is calculated using equation 27,

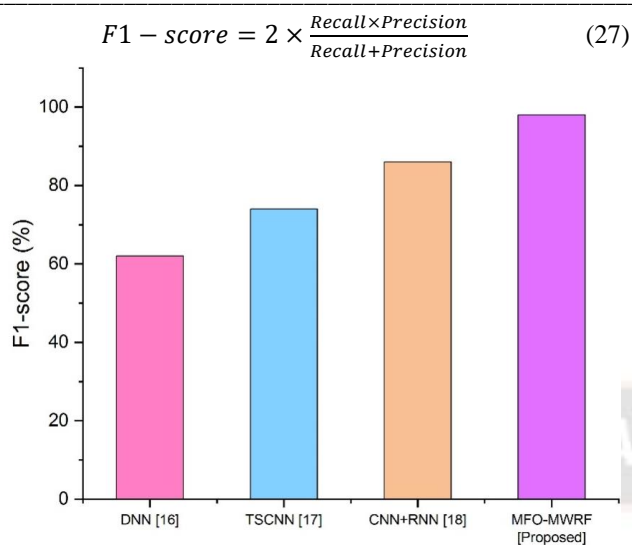


Figure 5: F1-Score

Fig 5 shows the f1-score of the proposed system. Recall consumption forecasts for both the current system and the suggested system are shown. The suggested method achieves 95% f1-source compared to 65% for DNN, 75% for TSCNN, and 85% for CNN+RNN. It demonstrates how successful the suggested strategy is than the current one.

V. CONCLUSION

This paper includes an effective MFO-MWRF-based framework for hybrid BCI signals classification. According to each governing brain-computer interface, the conceptual approach is capable of conducting analyses in hybrid BCI signals domains. The model is an automated framework that enables the evaluation of both DWT characteristics for WF processing issues. From this perceptive, it perfectly replicates a hybrid BCI signals expert's assessment procedure. The paper acquires both signal and noise features concurrently as opposed to obtaining information just as transform as previous approaches do. The MFO-MWRF component is thoroughly examined, and the parameters are chosen, to better illustrate the efficiency of each technique. According to the results, the suggested strategy performs better than the competition in solving the current hybrid BCI signals classification problem. Future studies will focus on the categorization of brain-computer interface signals at a greater level. Additionally, automated fixes will be made for problems brought on by composite signals with more than two signals.

REFERENCES

[1] S. Sadeghi, and A. Maleki, "A comprehensive benchmark dataset for SSVEP-based hybrid BCI," *Expert Systems with Applications*, vol. 200, pp.117180, 2022.

[2] R. Shelishiyah, M.B. Dharan, T.K. Kumar, R. Musaraf, and T.D. Beeta, "Signal Processing for Hybrid BCI Signals," In *Journal of Physics: Conference Series*, Vol. 2318, No. 1, pp. 012-007, Aug 2022, IOP Publishing.

[3] Z. Feng, Q. He, J. Zhang, L. Wang, X. Zhu, and M. Qiu, "A hybrid BCI system based on motor imagery and transient visual evoked potential," *Multimedia Tools and Applications*, vol. 79, pp.10327-10340, 2020.

[4] J. Choi, K.T. Kim, J.H. Jeong, L. Kim, S.J. Lee, and H. Kim, "Developing a motor imagery-based real-time asynchronous hybrid BCI controller for a lower-limb exoskeleton," *Sensors*, vol.20, no.24, pp.7309, 2020.

[5] L. Wang, X. Liu, Z. Liang, Z. Yang, Z. and X. Hu, "Analysis and classification of hybrid BCI based on motor imagery and speech imagery," *Measurement*, vol. 147, pp.106842, 2019.

[6] X. Cai, and J. Pan, "Toward a brain-computer interface-and internet of things-based smart ward collaborative system using hybrid signals," *Journal of Healthcare Engineering*, 2022.

[7] Yadav , A. K. ., Bhaskar Ch. , V. ., M., N. ., Raja, J. E. ., S. Pund, S. ., & Kumari , A. . (2023). A Secure Multi-Path Communication through Dynamic Path Identifiers to Prevent Denial-of-Service Flooding Attacks. *International Journal of Intelligent Systems and Applications in Engineering*, 11(3s), 22–28. Retrieved from <https://ijisae.org/index.php/IJISAE/article/view/2527>

[8] L.W. Ko, O. Komarov, and S. C. Lin, "Enhancing the hybrid BCI performance with the common frequency pattern in dual-channel EEG," *IEEE Transactions on Neural Systems and Rehabilitation Engineering*, vol. 27, no. 7, pp.1360-1369, 2019.

[9] Y. Wei, J. Li, H. Ji, L. Jin, L. Liu, Z. Bai, and C. Ye, "A Semi-Supervised Progressive Learning Algorithm for Brain-Computer Interface," *IEEE Transactions on Neural Systems and Rehabilitation Engineering*, vol. 30, pp.2067-2076, 2022.

[10] Z. Sun, Z. Huang, F. Duan, and Y. Liu, "A novel multimodal approach for hybrid brain-computer interface," *IEEE Access*, vol. 8, pp.89909-89918, 2020.

[11] D. Yang, T.H. Nguyen, and W.Y. Chung, "A bipolar-channel hybrid brain-computer interface system for home automation control utilizing steady-state visually evoked potential and eye-blink signals," *Sensors*, vol. 20, no.19, pp.5474, 2020.

[12] C. Chen, P. Zhou, A. N. Belkacem, L. Lu, R. Xu, X. Wang, W. Tan, Z. Qiao, P. Li, Q. Gao, and D. Shin, "Quadcopter robot control based on a hybrid brain-computer interface system," *Sensors and Materials*, vol. 32, no. 3, pp.991-1004, 2020.

[13] M.A. Hasan, M.U. Khan, and D. Mishra, "A computationally efficient method for hybrid EEG-fNIRS BCI based on the Pearson correlation," *BioMed Research International*, pp.1-13, 2020.

[14] Rajesh Kumar Chaudhary, M. K. C. (2021). The Role of School Management Towards Staff Motivation for Effective Performance in Nepal: During the Covid-19. *International Journal of New Practices in Management and Engineering*, 10(01), 01–11. <https://doi.org/10.17762/ijnpm.v10i01.93>

[15] Y. Zhang, S.Q. Xie, H. Wang, and Z. Zhang, "Data analytics in steady-state visual evoked potential-based brain-computer interface: A review," *IEEE Sensors Journal*, vol. 21, no. 2, pp.1124-1138, 2020.

[16] A. Chowdhury, A. Dutta, and G. Prasad, "Corticomuscular co-activation-based hybrid brain-computer interface for motor recovery monitoring," *IEEE Access*, vol. 8, pp.174542-174557, 2020.

- [17] V. Chamola, A. Vineet, A. Nayyar, and E. Hossain, "Brain-computer interface-based humanoid control: A review," *Sensors*, vol. 20, no. 13, pp.3620, 2020.
- [18] Christopher Davies, Matthew Martinez, Catalina Fernández, Ana Flores, Anders Pedersen. Machine Learning Approaches for Predicting Student Performance. *Kuwait Journal of Machine Learning*, 2(1). Retrieved from <http://kuwaitjournals.com/index.php/kjml/article/view/174>
- [19] M. Saadati, J. Nelson, and H. Ayaz, "Multimodal fNIRS-EEG classification using deep learning algorithms for brain-computer interfaces purposes," In *Advances in Neuroergonomics and Cognitive Engineering: Proceedings of the AHFE 2019 International Conference on Neuroergonomics and Cognitive Engineering, and the AHFE International Conference on Industrial Cognitive Ergonomics and Engineering Psychology*, July 24-28, 2019, Washington DC, USA vol. 10, pp. 209-220, 2019. Springer International Publishing.
- [20] W. Luo, W. Yin, Q. Liu, and Y. Qu, "A Hybrid Brain-Computer Interface Using Motor Imagery and SSVEP Based on Convolutional Neural Network," *arXiv preprint arXiv*, pp. 2212.05289, 2022.
- [21] A. Jayanthi, and E.C. Djamal, "Hybrid CNN-RNN in Motor Imagery Identification of Brain-Computer Interface," In *2021 8th International Conference on Advanced Informatics: Concepts, Theory, and Applications (ICAICTA)*, pp. 1-6, September 2021, IEEE.

